Internal oxidation process in diluted Fe–Cr alloys: a transmission Mössbauer spectroscopy study

R. Idczak[1]

Abstract The room-temperature study of $Fe_{0.97}Cr_{0.03}$ and $Fe_{0.94}Cr_{0.06}$ alloys was performed using the transmission Mössbauer spectroscopy (TMS). The TMS measurements allow to determine changes in chemical composition and content of iron oxides in the bulk of the studied samples during exposure to air at 570, 870 and 1070 K. The results indicate that the chemical composition of samples changes significantly, and it is strongly dependent on temperature at which the studied samples are exposed to air. The iron internal oxidation kinetics as well as the activation energies for the oxidation of iron atoms in studied alloys were calculated.

1 Introduction

Today, the nuclear energy sector is looking for new structural materials which could be able to keep their design parameters for a long time during the exposure to factors such as corrosion, high temperature and high-energy neutron bombardment. These conditions will exist in new types of advanced fission reactors (generation IV) and fusion reactors. One of the most interesting and promising types of structural materials which could be used in those innovative nuclear facilities is high-chromium ferritic/martensitic steels [1]. Many studies of iron–chromium alloys, which are the base components of high-chromium ferritic/martensitic steels, show that a certain amount of chromium makes an iron alloy corrosion resistant. At ambient conditions, a thin and transparent film of chromium oxide rapidly forms on the open surface of the alloy preventing further oxidation and blocking corrosion. Unfortunately, upon ageing the Fe–Cr alloys with high chromium content often undergo transformation to either a high-temperature σ phase or separation into Fe-rich (α) and Cr-rich (α') phases. These processes lead to significant degradation of mechanical properties of certain steel grades.

The main aim of this work is to expand the knowledge about corrosion process in Fe–Cr alloys with low chromium content at elevated temperatures. High-temperature corrosion is an important phenomenon which must be taken into account during designing of modern fission reactors such as the very-high-temperature reactor (VHTR) or the supercritical water reactor (SCWR). At the same time, for the Fe–Cr alloys with low chromium content the effect connected to separation into Fe-rich (α) and Cr-rich (α') phases should be negligible. In this work, the $Fe_{0.97}Cr_{0.03}$ and $Fe_{0.94}Cr_{0.06}$ alloys which were exposed to air at 570, 870 and 1070 K were investigated by the transmission Mössbauer spectroscopy (TMS). These measurements allow to compare the oxidation process in two Fe–Cr alloys with different chromium contents under the same oxidation conditions. On the basis of obtained TMS data, it is possible to determine the changes in chemical composition and content of iron oxides in studied alloys during exposure to air as well as calculate the iron internal oxidation kinetics and the activation energies for the internal oxidation of iron atoms. These parameters are crucial for better understanding a corrosion process of Fe–Cr alloys during exposure to air.

2 Experimental details

The samples of $Fe_{0.97}Cr_{0.03}$ and $Fe_{0.94}Cr_{0.06}$ alloys were prepared in an arc furnace. Appropriate amounts of the 99.98% pure iron and 99.995% pure chromium were

✉ R. Idczak
  ridczak@ifd.uni.wroc.pl

[1] Institute of Experimental Physics, University of Wrocław, pl. M. Borna 9, 50-204 Wrocław, Poland

melted into a water-cooled copper crucible in argon atmosphere and quickly cooled to room temperature. Solidified alloys were remelted two times to ensure homogeneity. The weight losses during the melting process were below 0.2% of the original weight, so the compositions of the obtained ingots were close to nominal ones. Resulting ingots were cold-rolled to the final thickness of about 0.035 mm. In the next step, $Fe_{0.97}Cr_{0.03}$ and $Fe_{0.94}Cr_{0.06}$ foils were annealed in the vacuum at 1270 K for 2 h. To obtain homogeneous and defect-free samples [2], after annealing process, the foils were slowly cooled to room temperature during 6 h. The annealed samples were exposed to air at 570, 870 and 1070 K for several hours. Each step of samples processing was followed by TMS measurements which were taken at room temperature by means of a constant-acceleration POLON spectrometer of standard design, using a 3.7-GBq ^{57}Co-in-Rh standard source with a full width at half maximum (FWHM) of 0.22 mm/s.

Each measured spectrum was fitted with a transmission integral for a sum of different six-line patterns corresponding to various isomer shifts *IS,* quadrupole splitting/shift *QS* as well as hyperfine fields *B* at ^{57}Fe nuclei generated by different chemical states of ^{57}Fe Mössbauer probes. The single-phase Fe–Cr alloy with bcc structure could be described by additive model which assumes that the influence of Cr atoms on *B* as well as the corresponding isomer shift *IS* on a subspectrum is additive and independent of the atom positions in the first two coordination shells of the nuclear probe [3]. In other words, it was accepted that for each subspectrum, the quantities *B* and *IS* are linear functions of the number *n* of Cr atoms located in the first two coordination shells of ^{57}Fe. The functions can be written as follows:

$$B(n) = B_0 + n\Delta B,$$
$$IS(n) = IS_0 + n\Delta IS, \tag{1}$$

where ΔB and ΔIS stand for the changes in *B* and *IS* with one Cr atom in the first two coordination shells of the Mössbauer probe. At the same time, it was assumed that the quadrupole splitting *QS* in a cubic lattice is equal to zero. All additional components which appeared in measured spectra were attributed to new compounds which were formed during exposure to air. Some of the obtained fits are presented in Figs. 1, 2, 3, 4, 5 and 6.

3 Results and discussion

As one can see in Figs. 1, 2, 3, 4, 5 and 6, the measured TMS spectra for $Fe_{0.97}Cr_{0.03}$ and $Fe_{0.94}Cr_{0.06}$ alloys change significantly with time of exposure to air. For samples exposed to air at 570 K for time shorter than 100 h, the TMS spectra analysis reveal existence of components (sextets) which could be assigned only to single-phase Fe–Cr alloy with bcc structure [3, 4]. For longer exposure time as well as for alloys exposed at 870 and 1070 K, the additional magnetically split components were observed.

Fig. 1 Room-temperature TMS spectra for the $Fe_{0.97}Cr_{0.03}$ sample exposed to air at 570 K for several hours, fitted with a sum of various number of *six-line patterns* corresponding to different chemical states of iron atoms
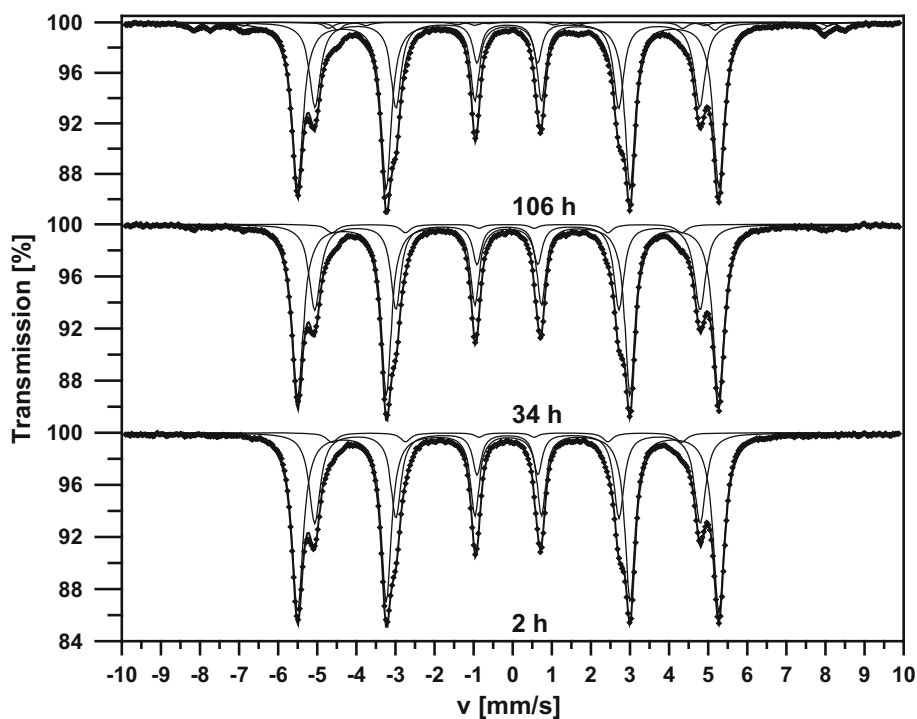
Fig. 2 Room-temperature TMS spectra for the $Fe_{0.97}Cr_{0.03}$ sample exposed to air at 870 K for several hours, fitted with a sum of five *six-line patterns* corresponding to different chemical states of iron atoms
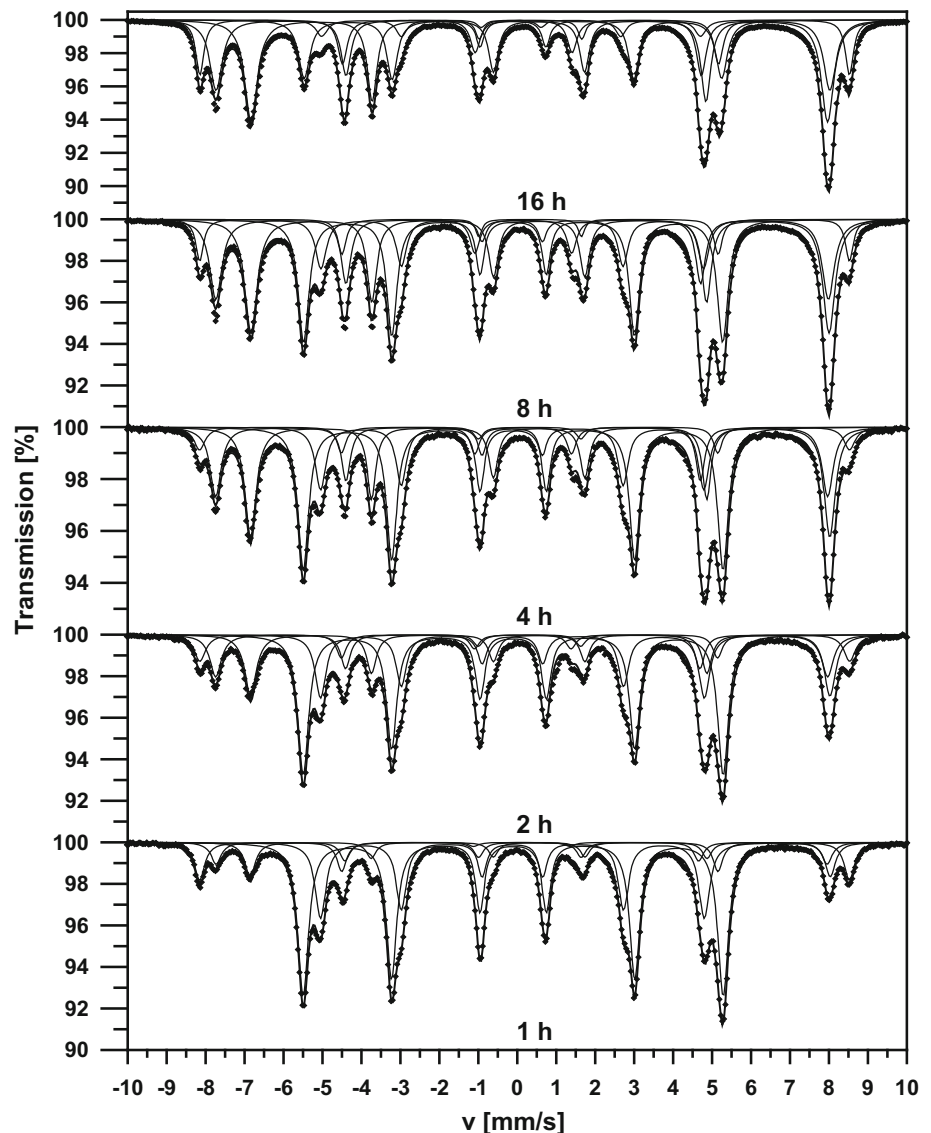

These subspectra were accounted for by adding to the model of the spectrum three sextets. One sextet with B $\approx$ 51.7 T, $IS \approx 0.37$ mm/s, $QS \approx -0.2$ mm/s could be a result of the α-Fe_2O_3 presence in the sample [5]. The last two sextets with B $\approx$ 48.9 T and 46.1 T, $IS \approx 0.24$ mm/s and 0.68 mm/s, $QS <$0.1 mm/s correspond to the two different sites of Fe atoms in Fe_3O_4 compound [6]. Here, it is worth noting that the changes in relative intensities of two Fe_3O_4 sextets were observed. This fact suggests that stoichiometric and non-stoichiometric Fe_3O_4 were formed [7, 8]. At the same time, in all measured TMS spectra, there are no other components which could be connected with FeO, FeOOH or iron carbides [9–11]. The obtained main hyperfine parameters derived from the TMS spectra for studied samples are listed in Tables 1, 2. The above findings are important evidence that in $Fe_{0.97}Cr_{0.03}$ and $Fe_{0.94}Cr_{0.06}$ alloys

exposed to air at elevated temperatures, only two types of compounds are formed: α-Fe_2O_3 and Fe_3O_4. Moreover, the further analysis of the TMS spectra parameters being the effective thicknesses $T_A(x)$ related to components of each spectrum can give detailed information about a chemical composition of studied samples. That is possible because the effective thicknesses are determined by the fractions $c(x)$ of absorbing atoms corresponding to the components under consideration, and the proper relationship can be expressed as follows:

$$T_A(x) = \sigma_0 t_A N f c(x), \tag{2}$$

where σ_0 is the maximal cross section for nuclear γ resonance absorption, t_A denotes the thickness of the absorber, N stands for the total number of resonant absorbing atoms ^{57}Fe per unit volume, and f is the Lamb–Mössbauer factor. Assuming that the relative ratio of the Lamb–Mössbauer

Fig. 3 Room-temperature TMS spectra for the $Fe_{0.97}Cr_{0.03}$ sample exposed to air at 1070 K for several hours, fitted with a sum of various number of *six-line patterns* corresponding to different chemical states of iron atoms
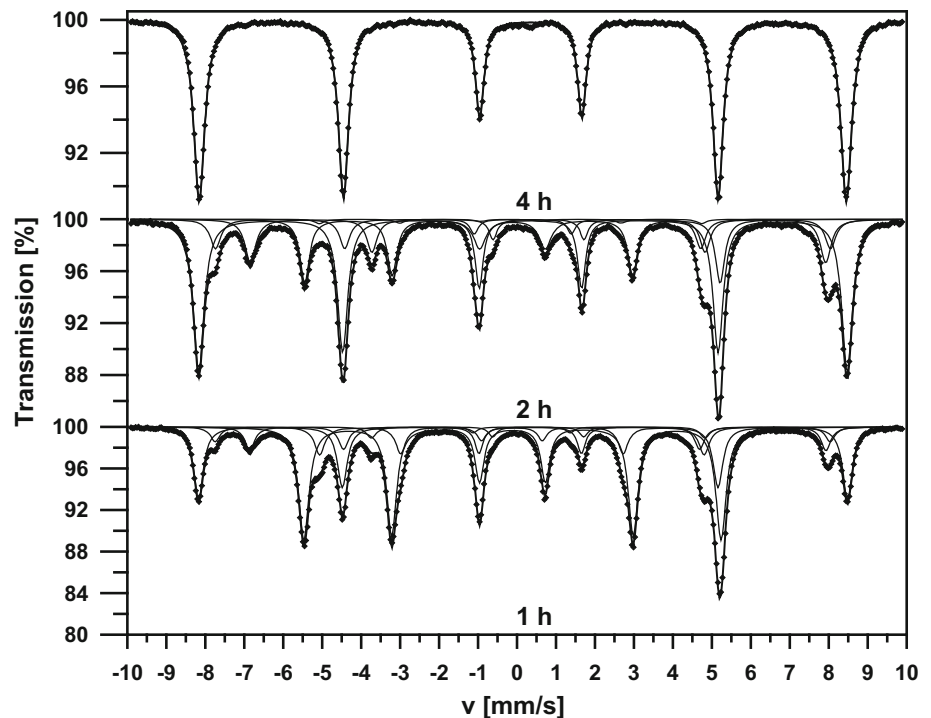
Fig. 4 Room-temperature TMS spectra for the $Fe_{0.94}Cr_{0.06}$ sample exposed to air at 570 K for several hours, fitted with a sum of various number of *six-line patterns* corresponding to different chemical states of iron atoms
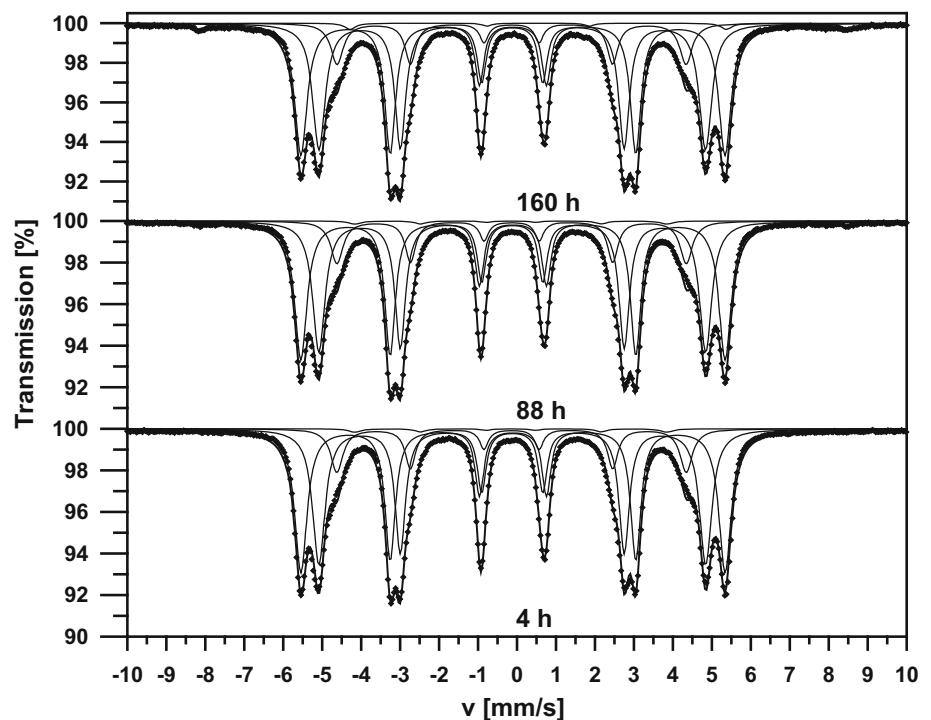

factors $f_{\alpha\text{-Fe}}:f_{\alpha\text{-Fe2O3}}:f_{Fe3O4}$ is equal to 1:1.08:1.05 [12], the fraction $c(x)$ can be easily calculated using the $T_A(x)$ values as in such case:

$$c(x) = \frac{T_A(x)}{\sum T_A(x)}. \tag{3}$$

The computed $c(x)$ values were used to find parameters $c(Fe)$, $c(Fe_2O_3)$ and $c(Fe_3O_4)$ which are the total intensities of spectrum components related to the existence of ^{57}Fe nuclear probes in α-Fe, α-Fe$_2$O$_3$ and Fe$_3$O$_4$, respectively. These parameters are listed in Tables 3, 4. Finally, to obtain a chemical composition of studied samples, it is

Fig. 5 Room-temperature TMS spectra for the $Fe_{0.94}Cr_{0.06}$ sample exposed to air at 870 K for several hours, fitted with a sum of six *six-line patterns* corresponding to different chemical states of iron atoms
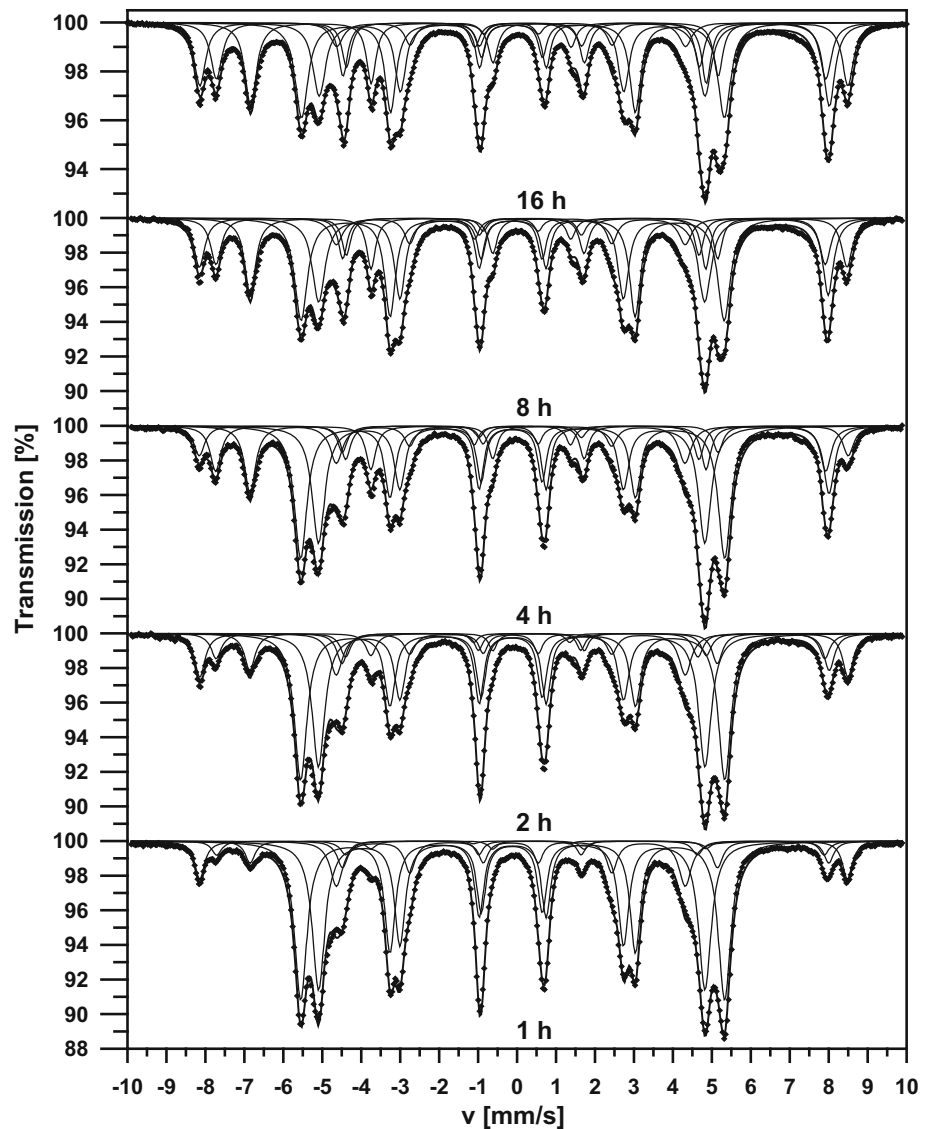
necessary to take into account that the relative quantities of iron atoms in observed compounds are different and equal to 1:2:3 for α-Fe, α-Fe_2O_3 and Fe_3O_4, respectively. The chemical composition estimated under above-mentioned assumptions for two exposure temperatures (870 and 1070 K) is presented in Fig. 7. As one can expect, a few atomic percent of Cr impurity dissolved in iron matrix has a significant influence on oxidation process of iron atoms in studied materials. The comparison of obtained data with results presented in previous work which concerns oxidation of pure iron [13] suggests that the internal oxidation of iron atoms in Fe–Cr alloys slows with increasing Cr content.

To analyse thermal oxidation of iron in Fe–Cr alloys, the Deal–Grove model was applied [14]. This model requires

that the oxidation of Fe follows a mechanism whereby a thin layer of oxide is formed by place exchange after adsorption has occurred with further oxidation occurring due to an electric field mechanism. The electric field is formed by electrons tunnelling from the metal to the adsorbed oxygen and is able to support ion transport through the place exchange and formed thin oxide layer enabling the oxide layer to increase in thickness. Due to fact that TMS technique is not sensitive for thin oxide layer (below 100 nm), the parabolic regime (for thick films) was assumed:

$$Fe_{OX}(t) = \sqrt{kt}, \tag{4}$$

where Fe_{OX} is a fraction of oxidised iron atoms in studied alloys at time t and k denotes the reaction rate constant which is equal to:

Fig. 6 Room-temperature TMS spectra for the $Fe_{0.94}Cr_{0.06}$ sample exposed to air at 1070 K for several hours, fitted with a sum of various number of *six-line patterns* corresponding to different chemical states of iron atoms
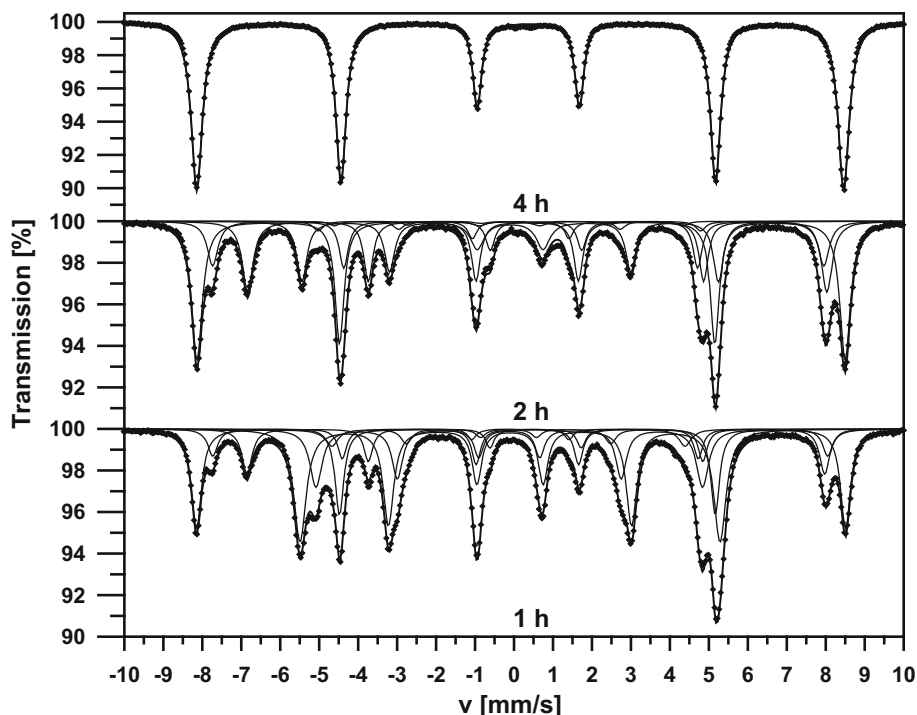
Table 1 Some parameters of the assumed model fitted to the room-temperature TMS spectra measured for $Fe_{0.97}Cr_{0.03}$ alloy exposed to air at 570, 870 and 1070 for several hours

t (h)	Bcc alloy				α-Fe_2O_3			Fe_3O_4 (Fe^{+3}) Fe_3O_4 ($Fe^{+2,+3}$)		
	B_0 (T)	IS_0 (mm/s)	ΔB (T)	ΔIS (mm/s)	B (T)	IS (mm/s)	QS (mm/s)	B (T)	IS (mm/s)	QS (mm/s)
570 K										
2	33.4	0.01	−2.8	−0.02	–	–	–	–	–	–
34	33.4	0.00	−2.8	−0.02	–	–	–	–	–	–
106	33.4	0.01	−2.9	−0.02	51.7	0.37	−0.19	48.5	0.20	0.03
								46.4	0.70	0.01
870 K										
1	33.4	0.01	−2.8	−0.02	51.7	0.37	−0.14	48.6	0.23	−0.01
								46.1	0.69	0.03
2	33.4	0.02	−2.9	−0.02	51.7	0.37	−0.12	48.7	0.25	−0.03
								46.1	0.70	0.03
4	33.4	0.02	−2.9	−0.02	51.7	0.37	−0.13	48.7	0.25	−0.04
								46.1	0.69	0.03
8	33.3	0.01	−2.9	−0.02	51.7	0.38	−0.14	48.7	0.26	−0.03
								46.0	0.69	0.02
16	33.2	0.01	−3.0	−0.04	51.7	0.39	−0.15	48.8	0.28	−0.02
								45.9	0.68	0.01
1070 K										
1	33.2	0.03	−2.7	−0.01	51.6	0.37	−0.18	48.9	0.25	0.03
								45.8	0.66	−0.01
2	33.0	0.03	−2.7	−0.05	51.6	0.37	−0.19	48.9	0.27	0.01
								45.7	0.67	−0.01
4	–	–	–	–	51.5	0.37	−0.21	–	–	–

The standard uncertainties for the parameters do not exceed 0.2 T for B, 0.04 mm/s for IS and 0.06 mm/s for QS. Values of the isomer shift IS are reported relative to the corresponding value for α-Fe at room temperature

Table 2 Some parameters of the assumed model fitted to the room-temperature TMS spectra measured for $Fe_{0.94}Cr_{0.06}$ alloy exposed to air at 570, 870 and 1070 for several hours

t (h)	Bcc alloy				α-Fe_2O_3			Fe_3O_4 (Fe^{+3}) Fe_3O_4 (Fe$^{+2,\,+3}$)		
	B_0 (T)	IS_0 (mm/s)	ΔB (T)	ΔIS (mm/s)	B (T)	IS (mm/s)	QS (mm/s)	B (T)	IS (mm/s)	QS (mm/s)
570 K										
4	33.7	0.02	−2.9	−0.02	–	–	–	–	–	–
88	33.7	0.02	−2.9	−0.02	–	–	–	–	–	–
160	33.7	0.02	−3.0	−0.02	51.7	0.41	−0.17	–	–	–
870 K										
1	33.7	0.01	−3.0	−0.02	51.5	0.37	−0.17	48.3	0.22	−0.03
								46.0	0.68	0.03
2	33.7	0.01	−3.0	−0.03	51.5	0.37	−0.15	48.4	0.22	−0.03
								46.1	0.68	0.02
4	33.7	0.01	−3.0	−0.03	51.6	0.38	−0.17	48.5	0.23	−0.04
								46.0	0.68	0.03
8	33.7	0.01	−3.0	−0.02	51.5	0.37	−0.18	48.5	0.24	−0.05
								46.0	0.68	0.02
16	33.6	0.02	−2.9	−0.02	51.5	0.38	−0.17	48.5	0.28	−0.05
								46.0	0.69	0.03
1070 K										
1	33.5	0.02	−2.8	−0.02	51.6	0.38	−0,16	48.9	0.28	0
								45.9	0.68	0.01
2	33.4	0.02	−2.8	−0.02	51.5	0.38	−0,16	48.6	0.26	−0.06
								46.1	0.70	0.03
4	–	–	–	–	51.4	0.38	−0,21	–	–	–

The standard uncertainties for the parameters do not exceed 0.2 T for B, 0.04 mm/s for IS and 0.06 mm/s for QS. Values of the isomer shift IS are reported relative to the corresponding value for α-Fe at room temperature

Table 3 Calculated from TMS spectra total intensities of components which are related to the existence of ^{57}Fe nuclear probes in $Fe_{0.97}Cr_{0.03}$ alloy, α-Fe_2O_3 and Fe_3O_4

Exposure time (h)	c (alloy) (%)	c (Fe_2O_3) (%)	c (Fe_3O_4) (%)
570 K			
2	100	0	0
10	100	0	0
34	100	0	0
106	94	3	3
870 K			
1	73	12	15
2	60	9	31
4	50	7	43
8	42	8	50
16	25	14	61
1070 K			
1	58	28	14
2	21	54	25
4	0	100	0

The standard uncertainties for the $c(x)$ parameters do not exceed 1%

Table 4 Calculated from TMS spectra total intensities of components which are related to the existence of ^{57}Fe nuclear probes in $Fe_{0.94}Cr_{0.06}$ alloy, α-Fe_2O_3 and Fe_3O_4

Exposure time (h)	c (alloy) (%)	c (Fe_2O_3) (%)	c (Fe_3O_4) (%)
570 K			
2	100	0	0
10	100	0	0
34	100	0	0
106	94	3	3
870 K			
1	85	8	7
2	74	11	16
4	66	8	26
8	59	12	29
16	51	15	34
1070 K			
1	56	26	18
2	22	43	35
4	0	100	0

The standard uncertainties for the $c(x)$ parameters do not exceed 1%
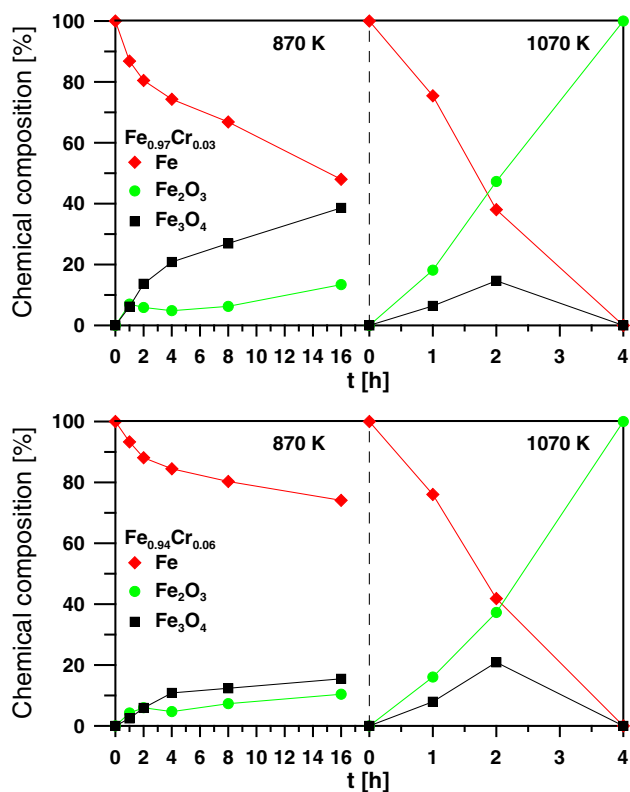
Fig. 7 Chemical composition of the $Fe_{0.97}Cr_{0.03}$ and $Fe_{0.94}Cr_{0.06}$ alloys exposed to air at 870 and 1070 K in function of exposure time

$$k = k_0 \exp\left(\frac{E_A}{k_B T}\right), \tag{5}$$

where E_A is activation energy for iron oxidation, k_B stands for Boltzmann constant, k_0 is pre-exponential factor, and T denotes temperature. Surprisingly, during analysis of the iron oxidation kinetic curves, it was found that parabolic regime is not valid and the logarithmic oxidation kinetics was much more plausible:

$$Fe_{OX}(t) = k \cdot \log(Ct + 1), \tag{6}$$

where k denotes a reaction rate constant and C is a constant. The parabolic and logarithmic iron oxidation kinetic curves fitted to experimental data obtained for the $Fe_{0.97}Cr_{0.03}$ and $Fe_{0.94}Cr_{0.06}$ alloys exposed to air at 870 and 1070 K are presented in Fig. 8. The knowledge of the reaction rate k, for two different temperatures, $T_1 = 870$ K and $T_2 = 1070$ K combined with Eq. (5), enabled determination of the activation energy E_A, for the oxidation of iron atoms in the temperature interval of 870–1070 K, using the following equation:

$$E_A = \frac{T_1 T_2}{T_2 - T_1} k_B \ln\left(\frac{k_2}{k_1}\right). \tag{7}$$

This equation is valid assuming that the pre-exponent factor k_0 in Eq. (5) is temperature independent. The
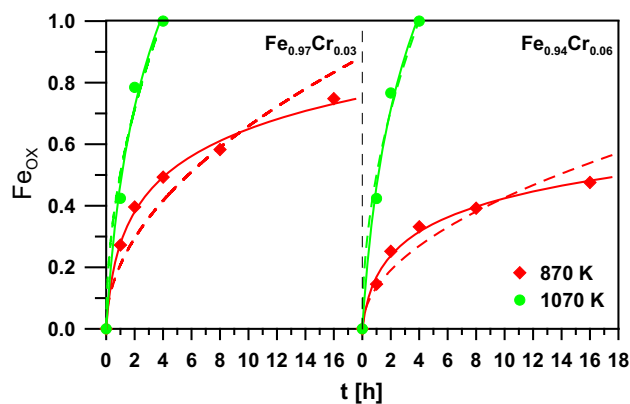
Fig. 8 Iron oxidation kinetics obtained for the $Fe_{0.97}Cr_{0.03}$ and $Fe_{0.94}Cr_{0.06}$ alloys exposed to air at 870 and 1070 K. The best fit to the data in terms of Eqs. (4) and (6) are indicated by a *dashed and solid lines*, respectively

Table 5 Estimated reaction rate constants k as well as activation energies of iron oxidation process E_A for studied Fe–Cr alloys

T (K)	k	E_A (eV)	E_A (kJ/mol)
$Fe_{0.97}Cr_{0.03}$			
870	0.41 (3)	0.46(2)	44(2)
1070	1.3 (4)		
$Fe_{0.94}Cr_{0.06}$			
870	0.29 (3)	0.60(3)	58(3)
1070	1.3 (3)		

estimated reaction rate constants as well as activation energies of iron internal oxidation process for studied Fe–Cr alloys are presented in Table 5. The obtained E_A values for Fe–Cr alloys are much higher than the activation energy for the oxidation reaction of pure Fe which was determined to be 32(6) kJ/mol [15]. This is in accord with the observation that the iron oxidation process in Fe–Cr alloys is much slower than the one in pure iron sample. Moreover, the higher E_A value for $Fe_{0.94}Cr_{0.06}$ alloy also agrees with previous conclusion that the internal oxidation of iron atoms slows with increasing Cr content.

4 Conclusions

The results reported in this paper can be concluded as follows:

1. The TMS measurements of $Fe_{0.97}Cr_{0.03}$ and $Fe_{0.94}Cr_{0.06}$ alloys allow to determine changes in chemical composition and the presence of newly formed compounds in studied materials during exposure to air at 570, 870 and 1070 K.

2. The comparison of data obtained for $Fe_{0.97}Cr_{0.03}$ and $Fe_{0.94}Cr_{0.06}$ samples results in conclusion that the internal oxidation of iron atoms slows with increasing Cr content.

3. It was found that parabolic regime for internal oxidation of iron atoms in diluted Fe–Cr alloys is not valid and the logarithmic oxidation kinetics was much more plausible.

4. The estimation of the reaction rate k, for two different temperatures, $T_1 = 870$ K and $T_2 = 1070$ K, enabled determination of the activation energy E_A for the internal oxidation of iron atoms in studied Fe–Cr alloys. $E_A = 0.46(2)$ eV for $Fe_{0.97}Cr_{0.03}$ and $E_A = 0.60(3)$ eV for $Fe_{0.94}Cr_{0.06}$.

References

1. I. Cook, Materials research for fusion energy. Nat. Mater. **5**, 77–80 (2006)

2. R. Idczak, R. Konieczny, J. Chojcan, A study of defects in iron-based binary alloys by the Mössbauer and positron annihilation spectroscopies. J. Appl. Phys. **115**, 103513 (2014)

3. I. Vincze, I.A. Campbell, Mössbauer measurements in iron base alloys with transition metals. J. Phys. F **3**, 647–663 (1973)

4. Rafał Idczak, Karolina Idczak, Robert Konieczny, Oxidation and surface segregation of chromium in Fe–Cr alloys studied by Mössbauer and X-ray photoelectron spectroscopy. J. Nucl. Mater. **452**, 141–146 (2014)

5. R. Zboril, M. Mashlan, D. Petridis, Iron(III) oxides from thermal processess synthesis, structural and magnetic properties, Mössbauer spectroscopy characterization, and applications. Chem. Mater. **24**, 969–982 (2002)

6. B.J. Evans, S.S. Hafner, ^{57}Fe hyperfine fields in magnetite (Fe_3O_4). J. Appl. Phys. **40**, 1411–1413 (1969)

7. J.M. Daniels, A. Rosencwaig, Mössbauer spectroscopy of stoichiometric and non-stoichiometric magnetite. J. Phys. Chem. Solids **30**, 156l–1571 (1969)

8. F.C. Voogt, T. Hibma, G.L. Zhang, M. Hoefman, L. Niesen, Growth and characterization of non-stoichiometric magnetite $Fe_{3-\delta}O_4$ thin films. Surf. Sci. **331–333**, 1508–1514 (1995)

9. L.F. Checherskaya, V.P. Romanov, P.A. Tatsienko, Mössbauer effect in Wüstite. Phys. Stat. Sol. a **19**, K177–K182 (1973)

10. F. Van der Woude, A.J. Dekker, Mössbauer Effect in α-FeOOH. Phys. Stat. Sol. **13**, 181–193 (1966)

11. B. Kniep, A. Constantinescu, D. Niemeier, K.D. Becke, An in situ Mössbauer Study of the Formation of Cementite, Fe_3C. Z. Anorg. Allg. Chem. **629**, 1795–1804 (2003)

12. D.A. Channing, M.J. Graham, A study of iron oxidation processes by mössbauer spectroscopy. Corros. Sci. **12**, 271–289 (1972)

13. K. Idczak, R. Idczak, R. Konieczny, An investigation of the corrosion of polycrystalline iron by XPS, TMS and CEMS. Phys. B **491**, 37–45 (2016)

14. B.E. Deal, A.S. Grove, General relationship for the thermal oxidation of silicon. J. Appl. Phys. **36**, 3770–3778 (1965)

15. A.P. Grosvenor, B.A. Kobe, N.S. McIntyre, Activation energies for the oxidation of iron by oxygen gas and water vapour. Surf. Sci. **574**, 317–321 (2005)